Research Article | Vol. 27, No. 26 / 23 December 2019 / Optics Express 38270

Optics EXPRESS

Optical Kerr effect and third harmonic generation in topological Dirac/Weyl semimetal

TIANNING ZHANG,[1] K. J. A. OOI,[2] WENCHAO CHEN,[3] L. K. ANG,[1,4] AND YEE SIN ANG[1,5]

[1] *Science and Math, Singapore University of Technology and Design, 8 Somapah Road, Singapore 487372, Singapore*
[2] *School of Energy and Chemical Engineering, Xiamen University Malaysia, Selangor Darul Ehsan 43900, Malaysia & College of Chemistry and Chemical Engineering, Xiamen University, Xiamen 361005, China*
[3] *Zhejiang University/University of Illinois Urbana-Champaign (ZJU/UIUC) Institute, International Campus, Zhejiang University, Haining 314400, China*
[4] *ricky_ang@sutd.edu.sg*
[5] *yeesin_ang@sutd.edu.sg*

Abstract: We study the nonlinear optical response generated by the massless Dirac quasiparticles residing around the topologically-protected Dirac/Weyl nodal points in three-dimensional (3D) topological semimetals. Analytical expressions of third-order interband nonlinear optical conductivities are obtained based on a quantum mechanical formalism which couples 3D Dirac fermions with multiple photons. Our results reveal that the massless Dirac fermions in three dimensions retains strong optical nonlinearity in terahertz frequency regime similar to the case of the two-dimensional Dirac fermions in graphene. At room temperature, the Kerr nonlinear refractive index and the harmonic generation susceptibility are found to be $n_2 = 10^{-11} \sim 10^{-8}$ m^2W^{-1} and $\chi^{(3)} = 10^{-14} \sim 10^{-8}$ m^2V^{-2}, respectively, in the few terahertz frequency regimes, which is comparable to graphene and orders of magnitudes stronger than many nonlinear crystals. Importantly, because 3D topological Dirac/Weyl semimetals possess bulk structural advantage not found in the strictly two-dimensional graphene, greater design flexibility and improved ease-of-fabrication in terms of photonic and optoelectronic device applications can be achieved. Our finding reveals the potential of 3D topological semimetals as a viable alternative to graphene for nonlinear optics applications.

1. Introduction

The discovery of topologically-protected emergent Dirac/Weyl nodal fermions in three-dimensional (3D) crystalline solids represents a major milestone of 21st century condensed matter physics and material science. Unlike graphene in which the (2 + 1) massless Dirac fermions is strictly confined in the atomically-thin two-dimensional (2D) plane of the hexagonal carbon lattice, the (3 + 1) massless Dirac fermions resides in the bulk of the 3D crystals and has a linear electronic band structure dispersing in all three dimensions at the vicinity of the Dirac/Weyl nodal point [1], [2]. The existence of such topologically-protected nodal point in the 3D crystal has been experimentally confirmed in Na_3Bi [3], Cd_2As_3 [4,5] and many other crystals. Immediately after the first experimental confirmation of 3D topological nodal point semimetals, many exotic physics phenomena such as chiral anomaly [6], transversal shift at a superconducting interface [7], large intrinsic anomalous Hall effect [8] and exceptionally strong magnetoresistance [9] have been subsequently identified. The extraordinarily rich physics contained in topological systems have fueled an extensive search of exotic topological emergent fermions in 3D solids, and the *zoo* of topological semimetals, such as Weyl fermions, nodal line, nodal surface, Hopf link, double helix, hourglass, and so on, continue to expand.

#375747 https://doi.org/10.1364/OE.27.038270
Journal © 2019 Received 21 Aug 2019; revised 9 Nov 2019; accepted 13 Nov 2019; published 17 Dec 2019

Optics EXPRESS

One of the hallmarks of the (2 + 1)-dimensional massless Dirac quasiparticles in graphene is their exceptionally strong optical nonlinearity that covers a rather broad frequency regime of far infrared, terahertz and near infrared [10–13]. The optical nonlinearity of graphene been extensively studied theoretically and experimentally in recent years. Graphene's nonlinear optical coefficient has been determined at around $n_2 = 10^{-11}$-$10^{-15} m^2/W$ around the visible and telecommunication spectrum by various experimental approaches, such as the four-wave-mixing (FWM) [14], self-phase modulation (SPM) [15], and Z-scan measurements [16–20]. Together with many unusual electronic and optical properties of graphene that arises from its unusual linear Dirac conic band structure, such as the tunable optical conductivity, strong light confinement, and the exceptionally high electrical mobility, graphene has been hailed as a promising holy grail for plasmonic applications [21,22]. More recently, the electrostatic-gate-tunable terahertz plasmon and third-order optical response have been demonstrated [23,24], thus opening up a new route of dynamically tunable nonlinear optical applications not achievable in conventional nonlinear media.

For the case of (3 + 1)-dimensional emergent Dirac fermions in topological Dirac/Weyl semimetals, the presence of linear Dirac conic band structure is expected to produce optical properties similar to that of graphene. The linear optical response of Dirac and Weyl semimetals has been studied in [25] based on the wave-vector- and frequency-dependent current-current response function approach. Using Kubo linear response theory, it is found that 3D Dirac/Weyl semimetals not only host Dirac surface plasmon polariton at their surface, their 3D bulk nature further allows the propagation of unusual electromagnetic modes in a waveguide geometry [25,26]. Multiple designs of 3D-Dirac-semimetal-based photonic devices, such as metasurfaces, photonic crystals, and broadband absorber, have been recently proposed. In the nonlinear regime, the semiclassical third-order nonlinear *intraband* optical conductivity of 3D massless Dirac fermions, formulated using perturbative Boltzmann transport theory, has been reported in a recent pilot study [27], and it is found that topological Dirac semimetal significantly outperforms in the Kerr nonlinearity and nonlinear switching performance. This finding immediately suggests an exciting opportunity of replicating the nonlinear plasmonics of graphene in 3D topological solids without being restricted by the two-dimensionality of graphene. The computational model used in [27], however, is incomplete by laking in account with the quantum mechanical *interband* optical transition, which is expected to play an important role especially when the photon energy is significantly larger than the Fermi level. In this work, we formulate the nonlinear optical conductivities of 3D massless Dirac fermions in the quantum mechanical *interband* regime. By coupling the 3D Dirac equation with an external electromagnetic field, analytical expressions of the high-order optical conductivities are perturbatively and recursively constructed through Floquet expansion [28–33]. We focus on the technologically important nonlinear phenomena, namely the third-order optical Kerr and high-harmonic generation effects, and calculate their corresponding nonlinear coefficients. Using Cd_3As_2 as an illustrative example, we show that the optical nonlinearity of (3 + 1)-dimensional massless Dirac fermion is comparable with the 2D counterpart in graphene, and is orders of magnitude stronger than many nonlinear crystals. Our finding suggests that 3D topological Dirac/Weyl semimetal simultaneously retains the 3D structural advantage of conventional bulk metals and the strong optical nonlinearity of Dirac quasiparticles, thus serving as a strong alternative material to graphene for the design and development of novel nonlinear photonic and optoelectronic devices operating in the terahertz frequency regime.

2. Theoretical formalism

The minimal effective model describing the (3 + 1)-dimensional massless Dirac fermions around a single Dirac/Weyl nodal point can be written as $H_{\mathbf{k}} = \sum_i \hbar \sigma_i v_i k_i$, where $i = x,\ y,\ z$ denotes the three orthogonal spatial coordinates, $\mathbf{k} = (k_x, k_y, k_z)$ is the quasi particle wave vector, and v_i

Optics EXPRESS

is the directional-dependent Fermi velocity. While this simplistic effective model captures the essential physics of 3D gapless Dirac cone in Dirac and Weyl semimetals, the unusual properties of Weyl quasiparticles, such as the presence of a topological axion term in the electrodynamics in a Weyl node and the contrasting optical properties between Type I and Type II Weyl nodes as well as the Weyl node separations [34,35], are not captured by this model, and shall form the subject of future works. The eigenstate and the energy dispersion of $H_{\mathbf{k}}$ can be solved from the time-independent Schrödinger equation, $H_{\mathbf{k}}\xi_{\mathbf{k}} = \varepsilon_{\mathbf{k}}\xi_{\mathbf{k}}$, which yields,

$$\varepsilon_{\mathbf{k}} = \hbar\sqrt{v_x^2k_x^2 + v_y^2k_y^2 + v_z^2k_z^2}, \tag{1}$$

and

$$\xi_{\mathbf{k}} = \begin{pmatrix} \cos(\theta/2) \\ e^{i\phi}\sin(\theta/2), \end{pmatrix} \tag{2}$$

where $\phi \equiv \tan^{-1}\left(v_xk_x/v_yk_y\right)$, and $\theta \equiv \cos^{-1}\left(\hbar v_zk_z/\varepsilon_{\mathbf{k}}\right)$

In the presence of an external electromagnetic field, the photon can be coupled to $H_{\mathbf{k}}$ by the minimal coupling scheme [32,36], $\mathbf{k} \rightarrow \mathbf{k} + e\mathcal{A}$, where $\mathcal{A} = e\mathbf{E}(t)/i\omega$ and $\mathbf{E}(t) = \mathbf{E}_0e^{i\omega t}$. Here we consider only the case when the Dirac/Weyl semimetals is under a continuous wavefront illumination. Without loss of generality, we assume that the external electric field is pointing in the x-direction The photon-dressed Hamiltonian of a Dirac/Weyl nodal point is expressed as

$$H_{\mathbf{k}}(t) = \hbar\begin{pmatrix} P_z & P_-+Ae^{i\omega t} \\ P_++Ae^{i\omega t} & -P_z \end{pmatrix}, \tag{3}$$

where $P_z \equiv v_zk_z$, $P_- \equiv v_xk_x - iv_yk_y$, $P_+ = v_xk_x + iv_yk_y$, $A \equiv v_x\mathcal{A}_x = v_xE_x/i\omega$, $\omega = 2\pi f$ is the angular frequency.

The time-dependent two-spinor eigenstates of Eq. (3) can be expressed as an expansion in the basis set,

$$\psi_{\mathbf{k}}(t) = \sum_{n=-\infty}^{\infty}\begin{pmatrix}\alpha_n \\ \beta_n\end{pmatrix}e^{in\omega t}e^{-i\frac{\varepsilon_{\mathbf{k}}}{\hbar}t}, \tag{4}$$

where (α_n, β_n) are n-th order spinor components that contains all information related to the strength of n-photon/electron coupling process. The spinor components in Eq. (4) can be obtained from solving the time-dependent Schrodinger equation, $i\hbar\partial\psi_{\mathbf{k}}(t)/\partial t = H\psi_{\mathbf{k}}(t)$. Due to the orthonormal relation of $e^{in\omega t}$, we obtain the *recursion relations* that couples the n-th order with $(n-1)$-th order spinor components,

$$\begin{aligned}(\varepsilon_{\mathbf{k}} - P_z - n\tilde{\omega})\alpha_n &= P_-\beta_n + A\beta_{n-1} \\ (\varepsilon_{\mathbf{k}} + P_z - n\tilde{\omega})\beta_n &= P_+\alpha_n + A\alpha_{n-1}.\end{aligned} \tag{5}$$

where $\tilde{\omega} = \hbar\omega$. The n-th order dynamical current density can be calculated by,

$$\begin{aligned}\mathbf{J}(t) &= \frac{ge}{(2\pi\hbar)^3}\int N_\beta^\mu(\varepsilon_{\mathbf{k}})\langle\hat{\mathbf{v}}\rangle d^3\mathbf{k} \\ &= \frac{ge}{(2\pi\hbar)^3}\frac{1}{v_xv_yv_z}\int N(P)\langle\hat{\mathbf{v}}\rangle d^3\mathbf{P},\end{aligned} \tag{6}$$

where g is the degeneracy factor ($g = 4$ for Cd_3As_2), $\hat{\mathbf{v}} = \hbar^{-1}\partial H_{\mathbf{k}}(t)/\partial\mathbf{k}$, $\langle\hat{\mathbf{v}}\rangle = \psi_{\mathbf{k}}^\dagger(t)\hat{\mathbf{v}}\psi_{\mathbf{k}}(t)$, $\hat{v}_i = v_i\sigma_i$, $N_\beta^\mu(\epsilon) = n_F(\epsilon,\mu,T) - n_F(-\epsilon,\mu,T) = \sinh(\epsilon/k_BT)/[\cosh(\epsilon/k_BT) + \cosh(\mu/k_BT)]$ is the interband thermal factor, μ is the fermi level and T is the temperature. Here $\mathbf{P} = (v_xk_x,\ v_yk_y,\ v_zk_z)$

Optics EXPRESS

and $\varepsilon_{\mathbf{k}} = \epsilon = |\mathbf{P}| = |(v_x k_x,\ y_y k_y v_z k_z)|$. Taking into account the anisotropic fermi velocity, the i-directional current density is

$$J_i(t) = \frac{ge}{(2\pi\hbar)^3}\frac{v_i}{v_j v_k}\sum_{\Lambda}\int d\epsilon N_{\beta}^{\mu}(\epsilon) j_{\Lambda}(\epsilon)\epsilon^2, \tag{7}$$

where $v_{i,\,j,\,k}$ denotes the three fermi velocity for the 3D material, and v_i is the velocity along the direction of electromagnetic field.

$$j_{\Lambda}(\epsilon) = \int \sin(\theta) d\theta d\phi \sum_{n,\,m}^{n+m=\Lambda} (\alpha_n^* \beta_m + \beta_n^* \alpha_m) e^{i(n-m)\omega t}, \tag{8}$$

the notation * denotes complex conjugation.

We now briefly describe the procedures for deriving the nonlinear optical conductivity from Eqs. (5) and (7) [32,36,37]. Firstly, the substitution of $\tilde{\omega} \to \tilde{\omega} + i\delta$ is made, where δ is a small smearing term added to (7) to ensure convergence. In the limit of $\delta \to 0$, the Sokhotski-Plemelj formula is used to obtain $J_x(t)$. The optical conductivity can then be calculated as $\boldsymbol{\sigma}(t) = \mathbf{J}(t)/\mathbf{E}(t)$. For $n = 0$, there is no incident photons, the recursive formula in Eq. (5) can be solved to give the zeroth order spinor components, i.e. $\alpha_0 = \cos(\theta/2)$, $\beta_0 = \sin(\theta/2)\, e^{i\phi}$, which is in agreement with the bare electron eigenstate obtained from the time-independent Schrodinger equation [see Eq. (2)]. For $n \geq 1$, the recursive relation in Eq. (5) can be decoupled as

$$\begin{aligned}
\alpha_n &= C_n \left\{ \varepsilon_{\mathbf{k}} e^{-i\phi} \alpha_{n-1} + \left[\varepsilon_{\mathbf{k}} \cos\left(\frac{\theta}{2}\right) - (n-1)\tilde{\omega} \right] \beta_{n-1} \right\} \\
\beta_n &= C_n \left\{ \varepsilon_{\mathbf{k}} e^{i\phi} \beta_{n-1} - \left[\varepsilon_{\mathbf{k}} \cos\left(\frac{\theta}{2}\right) + (n-1)\tilde{\omega} \right] \alpha_{n-1} \right\},
\end{aligned} \tag{9}$$

where $C_n = A/n\tilde{\omega}(n\tilde{\omega} - 2P)$. Finally, the higher-order spinor components can be recursively constructed using Eq. (9), and the optical current densities can be calculated using the methods described above. In this work, we focus on the single-photon linear response, the third-order single-frequency nonlinear response which corresponds the simultaneous absorption of two photons and the emission of one photon, and the third-order triple-frequency nonlinear response which corresponds to the simultaneous absorption of three photons. The schematic drawing of the linear and third-order nonlinear optical processes are shown in Fig. 1.

For linear optical response, the electrical current density can be calculated by combining the $n = 0$ and $n = 1$ spinor components, i.e.

$$\sigma_{inter}^{(1)} = \frac{ge^2}{24\pi\hbar}\frac{v_i}{v_j v_k}\omega N_{\beta}^{\mu}(\tilde{\omega}/2), \tag{10}$$

which is in agreement with the real part optical conductivity calculated using Kubo linear response theory [26]. As $\sigma_{inter}^{(1)} \propto \omega$, the diverging nature of $\sigma_{inter}^{(1)}$ when $\omega \to \infty$ does not satisfy the Titchmarsch Theorem [38]. Thus, the imaginary part cannot be directly computed using Kramers-Kronig relations. Instead, to calculate the linear refractive index n_1 and k_1, we evaluate the imaginary part of the linear conductivity directly based on the Kubo formula [26]

$$\sigma_I(\omega) = \sigma_0 \frac{v_i}{v_j v_k}\int_0^{\epsilon_C} \frac{N_{\beta}^{\mu}(\epsilon) - N_{\beta}^{\mu}(\tilde{\omega}/2)}{\tilde{\omega}^2 - 4\epsilon^2}\epsilon d\epsilon \tag{11}$$

where $\sigma_0 = \frac{e^2 g\omega}{3\pi^2\hbar}$ and ϵ_C is the cutoff energy beyond which the Dirac spectrum is no longer linear.

Optics EXPRESS

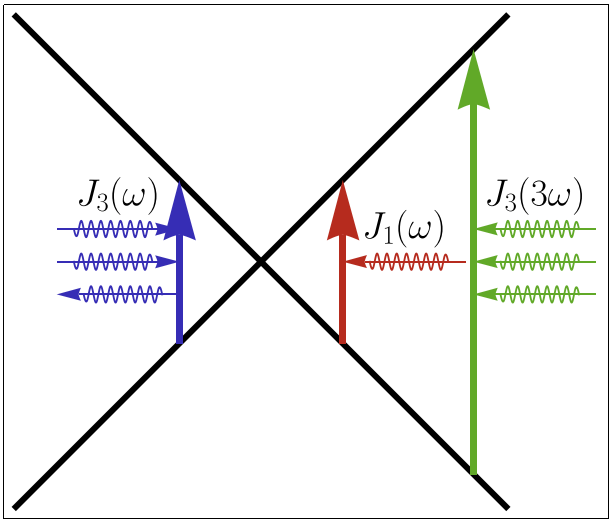

Fig. 1. Schematic illustration of linear and nonlinear optical processes in (3 + 1) massless Dirac fermions. For simplicity, we choose $k_x = k_y = 0$ plane. The first-order current is denoted by $J_1(\omega)$. The third-order terms are $J_3(\omega)$ and $J_3(3\omega)$. $J_3(\omega)$ corresponds to the Kerr process where two incoming photons are absorbed, followed by the immediate emission of a third photon. $J_3(3\omega)$ term corresponds to the simultaneous absorption of three photons that leads to high-harmonic generation.

The real part of the third-order optical conductivity is composed of two terms: (i) the single-frequency *Kerr* term; and (ii) the triple-frequency *high-harmonic generation* (HHG) term, which are found, respectively, as

$$\begin{aligned}\sigma^{(3)}_{inter}(\omega) &= \frac{ge^4v_i^3}{8\pi\hbar^3\omega^3}\frac{16}{15}N^{\mu}_{\beta}(\tilde{\omega})\\ \sigma^{(3)}_{inter}(3\omega) &= \frac{ge^4v_i^3}{8\pi\hbar^3\omega^3}\left[\frac{16}{45}N^{\mu}_{\beta}(\tilde{\omega}) - \frac{4}{45}N^{\mu}_{\beta}\left(\frac{\tilde{\omega}}{2}\right) - \frac{3}{5}N^{\mu}_{\beta}\left(\frac{3\tilde{\omega}}{2}\right)\right],\end{aligned} \tag{12}$$

We note that the nonlinear optical conductivity diverges as $\omega \to 0$. In this case, the carrier scattering effect becomes strongly dominant and a more comprehensive model that takes into account various carrier scattering mechanisms should be used. Thus, we have limited the minimum frequency to 0.1 THz so to avoid dwelling into the scattering-dominated regime. The imaginary part for the third-order nonlinear optical conductivity can be derived using the generalized Kramers-Kronig relations [38],

$$\omega^{\mathcal{N}}\sigma^{(n)}_{I}(\omega) = -\frac{1}{\pi}\int_{-\infty}^{\infty}\frac{\omega'^{\mathcal{N}}\sigma^{(n)}_{R}(\omega')}{\omega'-\omega}d\omega' \tag{13}$$

where $n = 1, 3$ for Kerr and HHG process, respectively. $\mathcal{N}$ is a correction factor that reduces the order of ω in the denominator of $\sigma^{(3)}_{inter}$ so to ensure the convergence of Eq. (13). For the case of Eq. (12), $\mathcal{N} = 3$. And for conventional Kramers-Kronig relations Eq. (13), $\mathcal{N} = 0$.

For completeness, we further include the semiclassical *intraband* optical conductivities, which has been previously developed in [27]. The intraband optical conductivities can be straightforwardly generalized to the case of anisotropic 3D Dirac cone, which is inevitably present in realistic topological Dirac semimetals such as Cd_3As_2. We obtain the following anisotropic

Optics EXPRESS

intraband optical conductivities,

$$\sigma^{(1)}_{intra}(\omega) = \frac{ge^2 v_i}{6\pi^2\hbar^3 v_j v_k}\frac{\tau}{1-i\omega\tau}\left[\mu^2 + \frac{\pi^2}{3}(k_B T)^2\right],$$
$$\sigma^{(3)}_{intra}(\omega) = \frac{ge^4 v_i^3}{5\pi^2\hbar^3 v_j v_k}\frac{\tau}{(1+\omega^2\tau^2)(1-2i\omega\tau)}\bar{n}_F, \tag{14}$$
$$\sigma^{(3)}_{intra}(3\omega) = \frac{3ge^4 v_i^3}{5\pi^2\hbar^3 v_j v_k}\frac{\tau}{(1-i\omega\tau)(1-2i\omega\tau)(1-3i\omega\tau)}\bar{n}_F,$$

where the $\bar{n}_F = [1+\exp(-\mu/k_B T)]^{-1}$ is the intraband thermal factor and we have assumed $\tau = 5$ ps as the carrier scattering time [39]. Finally, the total optical conductivity is evaluated as $\sigma = \sigma_{inter} + \sigma_{intra}$. In order to show its optical response, optical susceptibilities $\chi^{(n)}(\omega) = i\sigma^{(n)}/n\epsilon_0\omega$, as the factor to the polarization $P(t) = \epsilon_0[\chi^{(1)}E + \chi^{(2)}E^2 + \chi^{(3)}E^3 \ldots]$, is evaluated.

3. Results and discussions

The Cd_3As_2, as an illustrative example, has an anisotropic fermi velocity $(v_x, v_y, v_z) = (1.28, 1.30, 0.327)\times 10^6$ m/s. It's almost same along the x and y directions and significantly smaller along the z-direction. Because of this strong band structure anisotropy effect, the optical response is expected to be highly anisotropic. During calculation, we set the bandwidth of the linear energy dispersion to be $\epsilon_C \approx 0.1eV$.

In Fig. 2, the directional-dependent linear optical susceptibility is numerically evaluated in the frequency window between 0.1 THz and 10 THz. The vertical axis on the left and right-hand side denote the $x \approx y$ and z direction susceptibility, respectively. For the real part of the linear susceptibility, $\chi^{(1)}_R(\omega)$, the intraband component always dominates over the interband component. In contrast, for the imaginary part of the linear susceptibility, $\chi^{(1)}_I(\omega)$, the intraband component dominates over the interband only at low-frequency regime, while becomes significantly weaker than the interband component at a higher frequency. The difference between $x \approx y$ and z direction proportional to the velocity ratio $v_i^3/v_j v_k$, which leads to a significant deviation of approximately an order of magnitude between $\chi^{(3)}_{x\approx y}$ and $\chi^{(3)}_z$ in both real and imaginary parts. Due to inversion symmetry, the even-order nonlinear optical response is strictly forbidden.

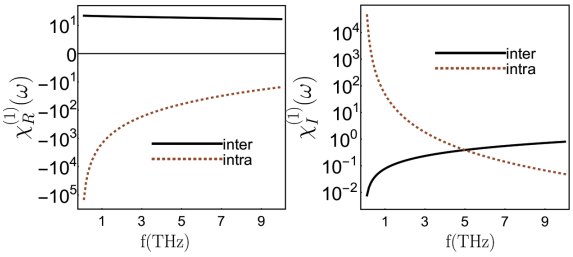

Fig. 2. Comparison between linear interband and intraband optical conductivity at $T = 300K$ and $\mu = 0.05eV$. Both the real and the imaginary parts of $\chi^{(1)}(\omega)$ along the x-and z-directions have the same frequency dependence but with different magnitude. The $\chi^{(1)}(\omega)$ along the x-direction is about 15 times large than that along the z-direction. (a) and (b) show the real and imaginary part of $\sigma^{(1)}(\omega)$, respectively.

The third-order nonlinear optical response is composed of two frequency modes, namely the single-frequency Kerr effect, $\chi^{(3)}(\omega)$, and the triple-frequency HHG process, $\chi^{(3)}(3\omega)$. The nonlinear susceptibilities are related to the nonlinear optical conductivities, $\sigma^{(3)}(\omega)$ and $\sigma^{(3)}(3\omega)$,

Optics EXPRESS

as

$$\chi^{(3)}(\omega) = i\frac{\sigma^{(3)}(\omega)}{\epsilon_0\omega} \quad , \quad \chi^{(3)}(3\omega) = i\frac{\sigma^{(3)}(3\omega)}{3\epsilon_0\omega}. \tag{15}$$

The Kerr and HHG susceptibilities are shown in Fig. 3. In general, the susceptibilities decay rapidly at a higher frequency due to the $1/\omega^4$ dependence. For the Kerr effect, a zero-value frequency exists, beyond which $\chi_R^{(3)}(\omega)$ changes from negative to a positive value. Such critical frequency signals a peculiar behavior at which the THz radiation propagating in a topological semimetal cross over from the self-focusing to the self-defocusing effect. In contrast, the HHG process, $\chi^{(3)}(3\omega)$, maintains a positive value throughout the THz regime. For the imaginary part, the HHG $\chi^{(3)}(3\omega)$ lies entirely in the negative regime, while the Kerr susceptibility exhibits a similar transition from positive to a negative value at low frequency. For higher fermi level, i.e. $\mu = 0eV, 0.01eV, 0.05eV$, the critical frequency, f_c, at which $\chi^{(3)}$ crosses over between the negative-valued and positive-valued regimes gradually shifts towards higher frequency. We further note that, at the typical values of $\mu = 0.01$ eV, the onset frequency of the interband optical response is estimated as $\omega = 2\mu/3\hbar \approx 10$ THz, which is beyond our frequency window of interests. Sharp optical transition due to interband process is thus not visible in our case.

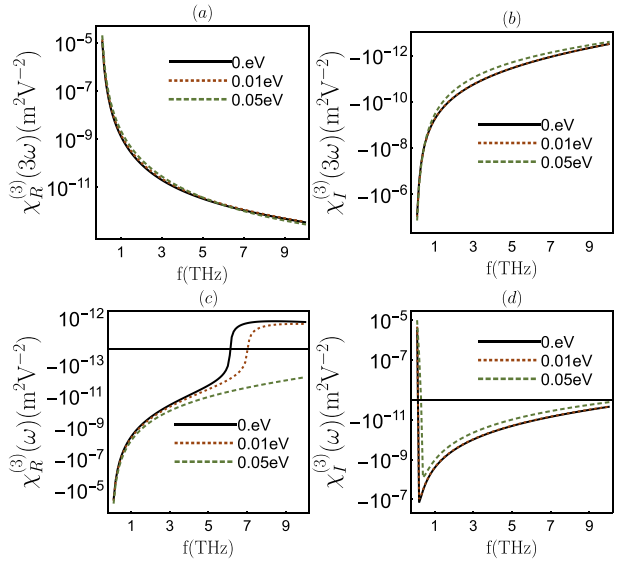

Fig. 3. Third-order nonlinear susceptibility at $T = 300$ K. (a) and (c) show the real part value of $\chi^{(3)}(\omega)$ for Kerr and HHG process, respectively. (b) and (d) shows the imaginary part corresponding to (a) and (c), respectively.

We further investigate the μ-dependence of the zero-value frequency in Fig. 4. It is seen that f_c increases monotonously with μ and almost linearly. This phenomena suggests that the self-focusing and self-defocusing effect can be flexibly tuned by using chemical or electrostatic doping, thus revealing potential applications of topological Dirac/Weyl semimetal in THz wave modulation.

Next we calculate the complex nonlinear refractive index, n_2 and k_2 by using the relations,

$$n + ik = \sqrt{1 + \chi^{(1)}}, \tag{16}$$

$$n_2 = \frac{3}{4\epsilon_0 c(n^2 + k^2)}[\chi_R^{(3)} + \frac{k}{n}\chi_I^{(3)}], \tag{17}$$

Optics EXPRESS

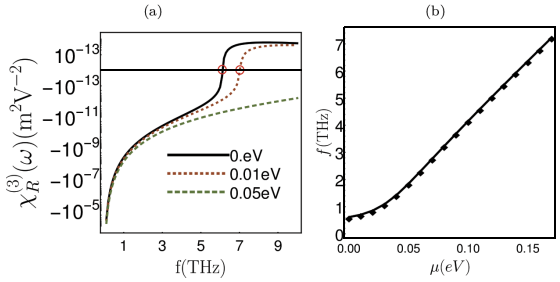

Fig. 4. The crossover effect from negative-valued to positive-valued $\chi^{(3)}(\omega)$. (a) The red circles highlight the critical frequency at which the crossover occurs. (b) shows the μ-dependence of the crossover frequency at $T = 300$ K.

$$k_2 = \frac{3}{4\epsilon_0 c(n^2 + k^2)}[\chi_I^{(3)} - \frac{k}{n}\chi_R^{(3)}]. \tag{18}$$

In Fig. 5, the n_2 and k_2 of the Kerr and HHG processes in the z-direction are shown. The cross-over from negative-valued to positive-valued occurs for both Kerr and HHG process [see Figs. 5(a) and 5(c)]. However, the k_2 behaves rather differently between the Kerr [Fig. 5(d)] and the HHG process [Fig. 5(b)]. For HHG, the k_2 is negative in the entire few THz window [Fig. 5(b)], while that of the Kerr process changes from positive value at low frequency to negative value at high frequency. This contrasting behaviors of k_2 shall provide a clear signature to distinguish between the Kerr and the HHG effects in topological Dirac/semimetal.

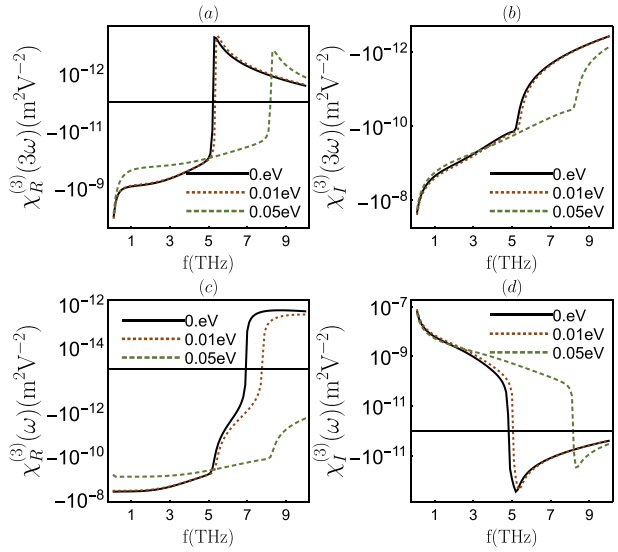

Fig. 5. The nonlinear refractive index along the z-direction at 300K. The Three type lines represent different chemical potentials condition. (a) and (b) shows the n_2 and k_2 of the HHG effect, respectively. (c) and (d) shows the n_2 and k_2 of the optical Kerr effect, respectively.

Due to the presence of anisotropic velocity in realistic 3D topological Dirac semimetal, the optical response becomes strongly anisotropic. In Fig. 6, the n_2 and k_2 of the Kerr and HHG processes along $x \approx y$ direction are shown. The n_2 [Figs. 6(a)] and k_2 [Figs. 6(b)] of the HHG process in $x \approx y$ direction remains qualitatively similar to that of the z direction. However, the n_2 of the Kerr process distinguish to the x [Fig. 6(c)] and z direction [Fig. 5(c)]. The crossover from

Optics EXPRESS

Kerr self-focusing to self-defocussing is no longer present in the few THz frequency windows along the x, y directions. The k_2 index of the Kerr process [Fig. 6(d)] remains qualitatively the same in all directions.

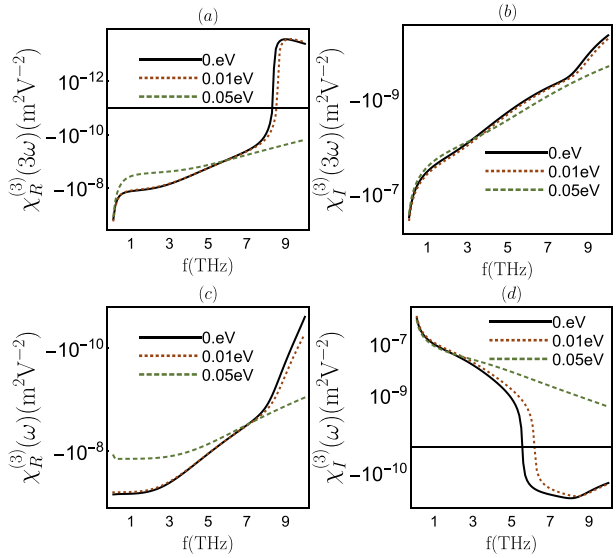

Fig. 6. The nonlinear refractive index along the x-direction at 300K. The Three type lines represent different chemical potentials condition. (a) and (b) shows the n_2 and k_2 of the HHG effect, respectively. (c) and (d) shows the n_2 and k_2 of the optical Kerr effect, respectively.

Finally, we compare the Kerr coefficients of Cd_3As_2 computed in this work with other nonlinear crystals. For $f \leq 5$ THz, the Kerr coefficient can reach around $|n_2| \approx 10^{-8} m^2 W^{-1}$, which is appreciably stronger than graphene [27] with $|n_2| \approx 10^{-10} m^2 W^{-1}$, Si_7N_3 with $|n_2| \approx 28 \times 10^{-18} m^2 W^{-1}$ [40], topological insulator Bi_2Se_3 with $|n_2| \approx 10^{-14} m^2 W^{-1}$ [41] and Bi_2Se_3-Bi_2Te_3 heterostructures with $|n_2| \approx 10^{-9}$ $10^{-10} m^2 W^{-1}$ [42], chalcogenide glass As_2S_3 with $|n_2| \approx 2.9 \times 10^{-18} m^2 W^{-1}$ [43], silicon with $|n_2| \approx 6 \times 10^{-18} m^2 W^{-1}$ [43] and silica with $|n_2| \approx 0.022 \times 10^{-18} m^2 W^{-1}$ [43].

4. Conclusion

In summary, we study the third-order nonlinear Kerr and HHG optical response generated by the 3D massless Dirac fermions in topological Dirac/Weyl semimetals. Using Cd_3As_2 as an illustrative example, we show that the optical nonlinearity of 3D topological semimetal can be comparable to graphene, and is significantly stronger than many other 3D crystals. The predicted nonlinear optical coefficients can be experimentally verified by measuring the terahertz waves high harmonic conversion efficiencies using intense terahertz pump pulse measurement [44]. Our model predicts a sharp transition from Kerr self-focusing to self-defocusing effect in few THz regimes, which shall form a clear smoking gun experimental signature of (3+1)-dimensional massless Dirac fermions. Importantly, the 3D nature of the topological Dirac/Weyl semimetal is more advantageous in terms of device fabrication and offers greater design flexibility compared to 2D graphene. Our findings thus reveal the potential of topological Dirac/Weyl semimetal as a promising candidate material for nonlinear Dirac photonic and optoelectronic applications.

Optics EXPRESS

Funding

A*STAR IRG (A1783c0011); Office of Naval Research Global (N62909-19-1-2047); ZJU-SUTD IDEA Grant; XMUM Research Fund (XMUMRF/2019-C3/IECE/0003); Ministry of Higher Education, Malaysia(FRGS/1/2019/TK08/XMU/02).

Acknowledgments

This work is supported by A*STAR IRG grant (A1783c0011) and ONRG grant (N62909-19-1-2047). YSA and WC acknowledge the support of ZJU-SUTD IDEA Grant. KJAO acknowledges the support of XMUM Research Fund, Grant No. XMUMRF/2019-C3/IECE/0003 and Fundamental Research Grant Scheme from the Ministry of Education Malaysia (FRGS/1/2019/TK08/XMU/02).

References

1. A. A. Burkov, M. D. Hook, and L. Balents, "Topological nodal semimetals," Phys. Rev. B **84**(23), 235126 (2011).
2. S. M. Young, S. Zaheer, J. C. Y. Teo, C. L. Kane, E. J. Mele, and A. M. Rappe, "Dirac semimetal in three dimensions," Phys. Rev. Lett. **108**(14), 140405 (2012).
3. Z. K. Liu, B. Zhou, Y. Zhang, Z. J. Wang, H. M. Weng, D. Prabhakaran, S.-K. Mo, Z. X. Shen, Z. Fang, X. Dai, Z. Hussain, and Y. L. Chen, "Discovery of a three-dimensional topological dirac semimetal, na3bi," Science **343**(6173), 864–867 (2014).
4. S. Borisenko, Q. Gibson, D. Evtushinsky, V. Zabolotnyy, B. Büchner, and R. J. Cava, "Experimental realization of a three-dimensional dirac semimetal," Phys. Rev. Lett. **113**(2), 027603 (2014).
5. M. Neupane, S.-Y. Xu, R. Sankar, N. Alidoust, G. Bian, C. Liu, I. Belopolski, T.-R. Chang, H.-T. Jeng, and H. Lin, "Observation of a three-dimensional topological dirac semimetal phase in high-mobility cd 3 as 2," Nat. Commun. **5**(1), 3786 (2014).
6. J. Xiong, S. K. Kushwaha, T. Liang, J. W. Krizan, M. Hirschberger, W. Wang, R. J. Cava, and N. P. Ong, "Evidence for the chiral anomaly in the dirac semimetal na3bi," Science **350**(6259), 413–416 (2015).
7. Y. Liu, Z.-M. Yu, and S. A. Yang, "Transverse shift in andreev reflection," Phys. Rev. B **96**(12), 121101 (2017).
8. K. Kuroda, T. Tomita, M.-T. Suzuki, C. Bareille, A. Nugroho, P. Goswami, M. Ochi, M. Ikhlas, M. Nakayama, and S. Akebi, "Evidence for magnetic weyl fermions in a correlated metal," Nat. Mater. **16**(11), 1090–1095 (2017).
9. C. Shekhar, A. K. Nayak, Y. Sun, M. Schmidt, M. Nicklas, I. Leermakers, U. Zeitler, Y. Skourski, J. Wosnitza, and Z. Liu, "Extremely large magnetoresistance and ultrahigh mobility in the topological weyl semimetal candidate nbp," Nat. Phys. **11**(8), 645–649 (2015).
10. S. Yamashita, "Nonlinear optics in carbon nanotube, graphene, and related 2d materials," APL Photonics **4**(3), 034301 (2019).
11. A. Singh, K. I. Bolotin, S. Ghosh, and A. Agarwal, "Nonlinear optical conductivity of a generic two-band system with application to doped and gapped graphene," Phys. Rev. B **95**(15), 155421 (2017).
12. A. Singh, S. Ghosh, and A. Agarwal, "Nonlinear and anisotropic polarization rotation in two-dimensional dirac materials," Phys. Rev. B **97**(20), 205420 (2018).
13. A. Singh, S. Ghosh, and A. Agarwal, "Terahertz shifted optical sideband generation in graphene," Phys. Rev. B **99**(12), 125419 (2019).
14. E. Hendry, P. J. Hale, J. Moger, A. Savchenko, and S. A. Mikhailov, "Coherent nonlinear optical response of graphene," Phys. Rev. Lett. **105**(9), 097401 (2010).
15. R. Wu, Y. Zhang, S. Yan, F. Bian, W. Wang, X. Bai, X. Lu, J. Zhao, and E. Wang, "Purely coherent nonlinear optical response in solution dispersions of graphene sheets," Nano Lett. **11**(12), 5159–5164 (2011).
16. H. Yang, X. Feng, Q. Wang, H. Huang, W. Chen, A. T. S. Wee, and W. Ji, "Giant two-photon absorption in bilayer graphene," Nano Lett. **11**(7), 2622–2627 (2011).
17. H. Zhang, S. Virally, Q. Bao, L. K. Ping, S. Massar, N. Godbout, and P. Kockaert, "Z-scan measurement of the nonlinear refractive index of graphene," Opt. Lett. **37**(11), 1856 (2012).
18. W. Chen, G. Wang, S. Qin, C. Wang, J. Fang, J. Qi, X. Zhang, L. Wang, H. Jia, and S. Chang, "The nonlinear optical properties of coupling and decoupling graphene layers," AIP Adv. **3**(4), 042123 (2013).
19. L. Miao, Y. Jiang, S. Lu, B. Shi, C. Zhao, H. Zhang, and S. Wen, "Broadband ultrafast nonlinear optical response of few-layers graphene: toward the mid-infrared regime," Photonics Res. **3**(5), 214 (2015).
20. T. Gu, N. Petrone, J. F. McMillan, A. van der Zande, M. Yu, G. Q. Lo, D. L. Kwong, J. Hone, and C. W. Wong, "Regenerative oscillation and four-wave mixing in graphene optoelectronics," Nat. Photonics **6**(8), 554–559 (2012).
21. K. J. A. Ooi and D. T. H. Tan, "Nonlinear graphene plasmonics," Proc. R. Soc. A **473**(2206), 20170433 (2017).
22. A. Grigorenko, M. Polini, and K. Novoselov, "Graphene plasmonics," Nat. Photonics **6**(11), 749–758 (2012).
23. B. Yao, Y. Liu, S.-W. Huang, C. Choi, Z. Xie, J. F. Flores, Y. Wu, M. Yu, D.-L. Kwong, and Y. Huang, "Broadband gate-tunable terahertz plasmons in graphene heterostructures," Nat. Photonics **12**(1), 22–28 (2018).
24. T. Jiang, D. Huang, J. Cheng, X. Fan, Z. Zhang, Y. Shan, Y. Yi, Y. Dai, L. Shi, and K. Liu, "Gate-tunable third-order nonlinear optical response of massless dirac fermions in graphene," Nat. Photonics **12**(7), 430–436 (2018).

Optics EXPRESS

25. A. Thakur, K. Sadhukhan, and A. Agarwal, "Dynamic current-current susceptibility in three-dimensional dirac and weyl semimetals," Phys. Rev. B **97**(3), 035403 (2018).
26. O. V. Kotov and Y. E. Lozovik, "Dielectric response and novel electromagnetic modes in three-dimensional dirac semimetal films," Phys. Rev. B **93**(23), 235417 (2016).
27. K. J. Ooi, Y. Ang, Q. Zhai, D. T. Tan, L. Ang, and C. Ong, "Nonlinear plasmonics of three-dimensional dirac semimetals," APL Photonics **4**(3), 034402 (2019).
28. Y. S. Ang and C. Zhang, "Enhanced optical conductance in graphene superlattice due to anisotropic band dispersion," J. Phys. D: Appl. Phys. **45**(39), 395303 (2012).
29. Y. S. Ang and C. Zhang, "Subgap optical conductivity in semihydrogenated graphene," Appl. Phys. Lett. **98**(4), 042107 (2011).
30. W. H. Cao and Y. S. Ang, "Effect of asymmetry on nonlinear optical response in graphene," Europhys. Lett. **107**(3), 37007 (2014).
31. S. Shareef, Y. S. Ang, and C. Zhang, "Room-temperature strong terahertz photon mixing in graphene," J. Opt. Soc. Am. B **29**(3), 274 (2012).
32. A. R. Wright, X. G. Xu, J. C. Cao, and C. Zhang, "Strong nonlinear optical response of graphene in the terahertz regime," Appl. Phys. Lett. **95**(7), 072101 (2009).
33. X. G. Xu, S. Sultan, C. Zhang, and J. C. Cao, "Nonlinear optical conductance in a graphene pn junction in the terahertz regime," Appl. Phys. Lett. **97**(1), 011907 (2010).
34. M. Kargarian, M. Randeria, and N. Trivedi, "Theory of kerr and faraday rotations and linear dichroism in topological weyl semimetals," Sci. Rep. **5**(1), 12683 (2015).
35. K. Sonowal, A. Singh, and A. Agarwal, "Giant optical activity and kerr effect in type-i and type-ii weyl semimetals," Phys. Rev. B **100**(8), 085436 (2019).
36. Z. Liu, C. Zhang, and J. C. Cao, "Nonlinear optical conductivity resulting from the local energy spectrum at the M point in graphene," Phys. Rev. B **96**(3), 035206 (2017).
37. Y. S. Ang, S. Sultan, and C. Zhang, "Nonlinear optical spectrum of bilayer graphene in the terahertz regime," Appl. Phys. Lett. **97**(24), 243110 (2010).
38. V. Lucarini, J. J. Saarinen, K.-E. Peiponen, and E. M. Vartiainen, *Kramers-Kronig relations in optical materials research*, vol. 110 (Springer Science & Business Media, 2005).
39. C. Zhu, F. Wang, Y. Meng, X. Yuan, F. Xiu, H. Luo, Y. Wang, J. Li, X. Lv, and L. He, "A robust and tuneable mid-infrared optical switch enabled by bulk dirac fermions," Nat. Commun. **8**(1), 14111 (2017).
40. K. Ooi, D. Ng, T. Wang, A. Chee, S. Ng, Q. Wang, L. Ang, A. Agarwal, L. Kimerling, and D. Tan, "Pushing the limits of cmos optical parametric amplifiers with usrn: Si 7 n 3 above the two-photon absorption edge," Nat. Commun. **8**(1), 13878 (2017).
41. S. Lu, C. Zhao, Y. Zou, S. Chen, Y. Chen, Y. Li, H. Zhang, S. Wen, and D. Tang, "Third order nonlinear optical property of bi 2 se 3," Opt. Express **21**(2), 2072–2082 (2013).
42. Q. Wang, X. Wu, L. Wu, and Y. Xiang, "Broadband nonlinear optical response in bi2se3-bi2te3 heterostructure and its application in all-optical switching," AIP Adv. **9**(2), 025022 (2019).
43. L. Thylen, P. Holmström, L. Wosinski, B. Jaskorzynska, M. Naruse, T. Kawazoe, M. Ohtsu, M. Yan, M. Fiorentino, and U. Westergren, "Chapter 6 - nanophotonics for low-power switches," in *Optical Fiber Telecommunications (Sixth Edition)*, I. P. Kaminow, T. Li, and A. E. Willner, eds. (Academic, Boston, 2013), Optics and Photonics, pp. 205–241, 6th edition ed.
44. H. A. Hafez, S. Kovalev, J.-C. Deinert, Z. Mics, B. Green, N. Awari, M. Chen, S. Germanskiy, U. Lehnert, and J. Teichert, "Extremely efficient terahertz high-harmonic generation in graphene by hot dirac fermions," Nature **561**(7724), 507–511 (2018).